Int J Appl Earth Obs Geoinformation 73 (2018) 786–799

Contents lists available at ScienceDirect

Int J Appl Earth Obs Geoinformation

journal homepage: www.elsevier.com/locate/jag

A satellite stand-alone procedure for deriving net radiation by using SEVIRI and MODIS products

J.M. Ramírez-Cuesta[a], D. Vanella[b,*], S. Consoli[b], A. Motisi[c], M. Minacapilli[c]

[a] Dpto. Riego, Centro de Edafología y Biología Aplicada del Segura (CEBAS-CSIC), P.O. Box 164, 30100 Murcia, Spain
[b] Dipartimento di Agricoltura, Alimentazione e Ambiente (Di3A), Università degli Studi di Catania, Via S. Sofia, 100, 95123 Catania, Italy
[c] Dipartimento di Scienze Agrarie e Forestali (SAF), Università degli Studi di Palermo, V.le delle Scienze Ed. 4, 90128, Palermo, Italy

ARTICLE INFO

Keywords:
Net radiation
MODIS
MSG-SEVIRI
FLUXNET
Vegetation characteristics

ABSTRACT

In this study, a new stand-alone satellite approach for the estimation of net surface radiation (R_n) has been implemented and validated for the Italian territory. The method uses the MODIS and MSG-SEVIRI time series products and it is independent of the use of ancillary data (i.e. ground measurements). A database of daily measurements of R_n, provided by 9 stations of the FLUXNET network, was used to validate the method in different ecological scenarios in the period 2010-12.

The R_n modelled by the proposed approach and the corresponding FLUXNET measurements were in good agreement, with RMSE and R^2 of 19.8 Wm^{-2} and 0.87, respectively, at 8-days scale, and 23.3 Wm^{-2} and 0.92, respectively, at daily scale.

Therefore, the proposed approach can be considered effective for the estimation of spatial and temporal variability of R_n, which is a key variable related to the management of water resources, agriculture, ecology and climate change.

1. Introduction

Net surface radiation (R_n) is the main driver for energy balance involved Earth processes, encompassing the total energy available for most of physical and biological activities (Carmona et al., 2015; Pan et al., 2015; Soltani et al., 2017). In numerical terms, R_n consists of the sum of 4 components: the downward/incoming short ($R_{ss\downarrow}$) and long ($R_{sl\downarrow}$) wave radiation and the upward/outgoing long ($R_{sl\uparrow}$) and short ($R_{ss\uparrow}$) wave radiation. An accurate determination of R_n is critical for the assessment of R_n-dependent processes (such as evapotranspiration, ET), since any error in its estimation will derive in miscalculations. R_n calculation is not an easy task, since multiple time and space changing atmospheric and land surface parameters are involved in it, including surface albedo (α), surface emissivity (ε_0), and land surface temperature (T_s).

Traditionally, R_n has been measured using field instruments (such as, pyrradiometer, pyranometer, pyrgeometer and net radiometer). Several ground-based networks for radiation measurements are spread around the world, as Global Energy Balance Archive (GEBA, Ohmura et al., 1989; Gilgen and Ohmura, 1999); Word Radiation Monitoring Center - Baseline Surface Radiation Network (WRMC-BSRN, Ohmura et al., 1998); Surface Radiation Budget Network (SURFRAD, Augustine et al., 2000, 2005); and FLUXNET (Baldocchi et al., 2001). In particular, GEBA is a database for surface energy fluxes measurements, maintained by the Institute for Climate and Atmospheric Sciences at ETH Zurich. It contains more than 2500 stations worldwide distributed, providing monthly averages of the surface energy balance components. BSRN became operational in 1992 and it consists on 48 stations placed all around the world in different climatic zones that provide observations of the short- and long-wave surface radiation fluxes with a high sampling rate. Established in 1993, SURFRAD is composed by 7 operational stations that provide long-term measurements of the surface radiation budget over the United States. FLUXNET global network consists of more than 500 micro-meteorological tower sites that measure the exchanges of carbon dioxide, water vapour, and surface energy fluxes between terrestrial ecosystems and the atmosphere.

Nevertheless, the data provided by ground measurements refers only to point-scale and their quality is greatly affected by instrumental error and/or maintenance faults (uncorrected sensor configurations or calibration), and land surface and atmosphere heterogeneities (Llasat

* Corresponding author.
E-mail address: d.vanella@unict.it (D. Vanella).

https://doi.org/10.1016/j.jag.2018.08.018
Received 20 March 2018; Received in revised form 27 June 2018; Accepted 17 August 2018
0303-2434/ © 2018 Elsevier B.V. All rights reserved.

Table 1
Summary of the spatial and temporal information of MODIS and SEVIRI products used in this study.

Data input	Sensor	Pixel size (km)	Temporal resolution	
			Daily	8-day
T_s (day-night), ε_o	MODIS	1	MOD11 A1	MOD11 A2
α		0.5		MCD43A3
$R_{ss\downarrow}$	SEVIRI	4	DIDSSF LSA-09	
$R_{sl\downarrow}$			DIDSLF LSA-12	

Table 2
FLUXNET data availability (X) within Italy region into the reference period 2010–12.

Site Code	Site Name	2010	2011	2012
IT-CA1	Castel d'Asso 1			X
IT-CA2	Castel d'Asso 2			X
IT-CA3	Castel d'Asso 3			X
IT-Col	Collelongo	X	X	X
IT-Lav	Lavarone	X	X	X
IT-MBo	Monte Bondone	X	X	X
IT-Ren	Renon	X	X	
IT-Ro2	Roccarespampani 2	X	X	
IT-Ro4	Roccarespampani 4			X

and Snyder, 1998; Wilson et al., 2002; Foken et al., 2006; Foken, 2008; Jacobs et al., 2008). In addition, it is difficult to extend the measurements made at specific locations up to regional scales (Blad et al., 1998), due to the strong influence of surface heterogeneity. Despite these limitations, the quality assurance and the data quality control performed at these networks allow their use for validating and evaluating satellite-based estimates of surface radiative fluxes.

Unlike ground-based observations, remotely sensed observations have the advantage of global coverage. In the last decades, a wide number of radiation products derived from satellite has been developed, highlighting: Earth Radiation Budget Experiment (ERBE, Smith et al., 1977; Jacobowitz et al., 1979, 1984; Barkstrom and Smith, 1986); Clouds and the Earth's Radiant Energy System (CERES, Wielicki et al., 1998); International Satellite Cloud Climatology Project (ISCCP, Zhang et al., 2004); Geostationary Earth Radiation Budget Project (GERB, Harries et al., 2005); and Surface Radiation Budget project (SRB, Cox et al., 2006). In addition, several surface radiation products have been derived from multispectral sensors such as Spinning Enhanced Visible and Infrared Imager (SEVIRI) aboard METEOSAT Second Generation (MSG) satellites; Visible Infrared Spin Scan Radiometer (VISSR) and Advanced Baseline Imager (ABI) on board Geostationary Operational Environmental Satellites (GOES); and Moderate Resolution Imaging Spectroradiometer (MODIS) aboard TERRA and AQUA satellites. However, one of the main limitation of approaches estimate R_n by using satellite data is that they usually requires ancillary data (i.e. ground measurements, such as maximum and minimum air temperature).

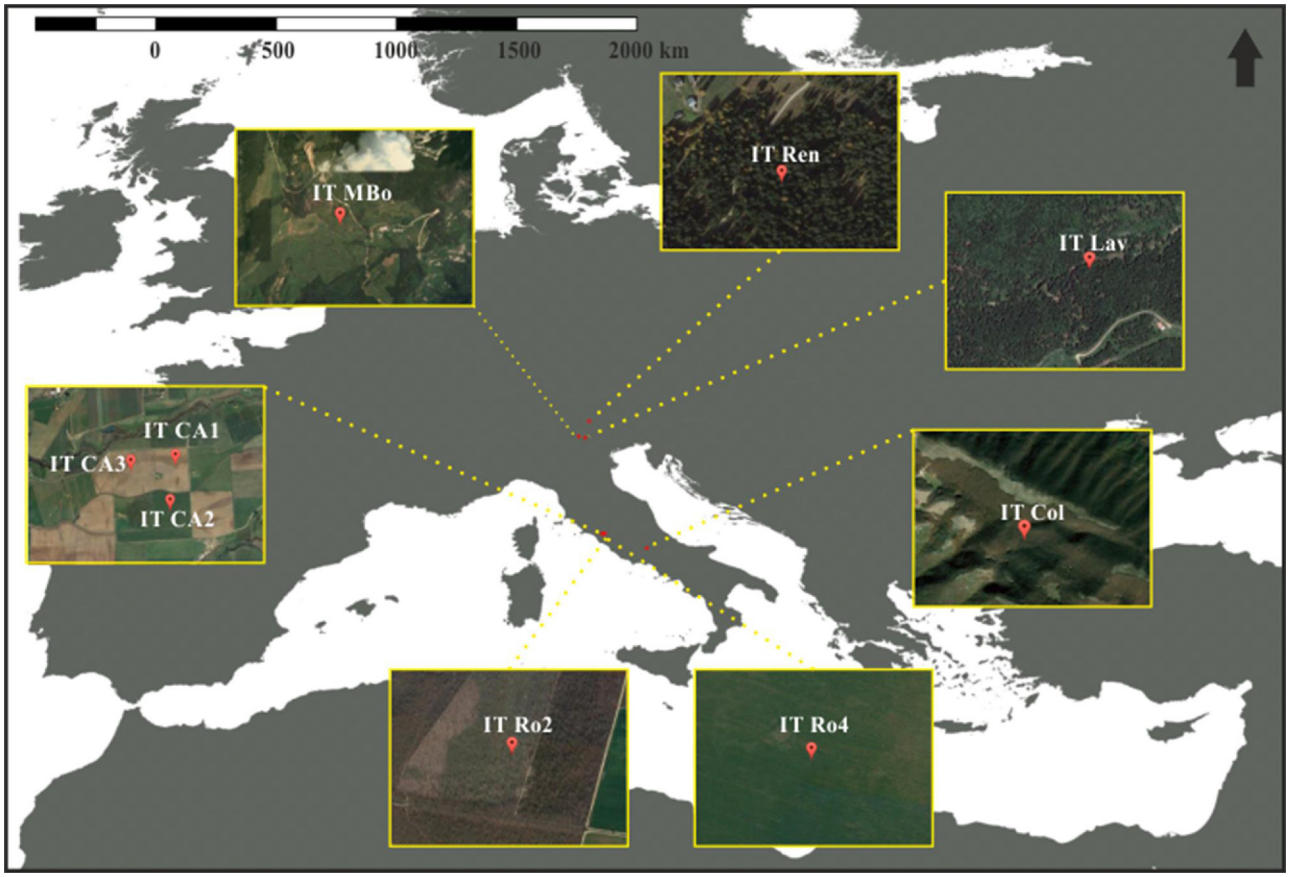

Fig. 1. FLUXNET sites selected in the study area within the reference period 2010–12.

Table 3
Summary on the FLUXNET sites information used in this study.

Site Code	Lat.(1)	Long.(2)	T_m(3)	P(4)	WD(5)	Slope (%)	Exposure	Elev.(6)	Landuse
IT-CA1	42.38	12.02	14	766	SW	Flat	Flat	200	Deciduous Broadleaf Forest
IT-CA2	42.38	12.02	14	766	SW	Gentle (< 2)	SW	200	Cropland
IT-CA3	42.38	12.02	14	766	SW	Flat	Flat	197	Cropland
IT-Col	41.85	13.59	6.3	1180	–	Undulated/Variable	S-SW	1560	Deciduous Broadleaf Forest
IT-Lav	45.96	11.28	7.8	1291	–	–	–	1353	Evergreen Needleleaf Forest
IT-MBo	46.01	11.04	5.1	1214	–	Flat	Flat	1550	Grassland
IT-Ren	46.59	11.43	4.7	809.3	NS	Strong (> 10)	NE-SW	1730	Evergreen Needleleaf Forest
IT-Ro2	42.39	11.92	15.15	876.2	–	–	–	160	Deciduous Broadleaf Forest
IT-Ro4	42.37	11.91	15.15	876	–	–	–	–	Cropland

Footnote for Table 3: (1) latitude, decimal degree (DD); (2) longitude, (DD); (3) mean annual temperature (°C); (4) mean annual precipitation (mm); (5) prevailing wind direction; (6) elevation (m., a.s.l.).

Table 4
FLUXNET measurements selected for the comparison with daily average R_n from satellite.

Winter (Dec – Feb)			Spring (Mar – May)			Summer (Jun – Aug)			Autumn (Sep – Nov)		
ID station	Date	DOY	ID station	Date	DOY	ID station	Date	DOY	ID station	Date	DOY
IT-Col	01/01/2012	1	IT-Col	01/03/2012	61	IT-Col	12/06/2011	163	IT-Ro2	01/09/2010	244
IT-Ro4	01/01/2012	1	IT-Lav	01/03/2012	61	IT-Ren	22/06/2011	173	IT-Ren	01/09/2010	244
IT-Ren	02/01/2011	2	IT-Ren	08/03/2011	67	IT-Ren	03/07/2011	184	IT-Col	01/09/2010	244
IT-Lav	08/01/2012	8	IT-Lav	09/03/2012	69	IT-Ro2	03/07/2011	184	IT-Ro2	02/09/2010	245
IT-Lav	12/01/2012	12	IT-Ro4	09/03/2012	69	IT-Ren	16/07/2010	197	IT-Col	02/09/2010	245
IT-Ro4	12/01/2012	12	IT-Ren	20/03/2011	79	IT-Ro2	16/07/2010	197	IT-Ro2	02/09/2011	245
IT-Col	15/01/2011	15	IT-Lav	31/03/2012	91	IT-Col	18/07/2011	199	IT-Col	11/09/2011	254
IT-Ro2	15/01/2011	15	IT-Ro4	31/03/2012	91	IT-Ren	26/07/2010	207	IT-Col	17/09/2011	260
IT-Ren	30/01/2011	30	IT-Ren	09/04/2011	99	IT-Ren	30/07/2010	211	IT-Ro2	17/09/2011	260
IT-Col	14/02/2011	45	IT-Col	09/04/2011	99	IT-Ro2	30/07/2010	211	IT-Ren	28/09/2011	271
IT-Ren	14/02/2011	45	IT-Ro2	09/04/2011	99	IT-Ren	31/07/2010	212	IT-Col	28/09/2011	271
IT-Ro2	01/12/2011	335	IT-Ren	26/04/2011	116	IT-Col	01/08/2011	213	IT-Col	29/09/2010	272
IT-Col	01/12/2011	335	IT-Ro2	11/05/2011	131	IT-Ro2	12/08/2011	224	IT-Ren	29/09/2010	272
IT-Ren	01/12/2011	335	IT-Lav	10/05/2012	131	IT-Ro2	22/08/2011	234	IT-Ro2	29/09/2010	272
IT-Ro2	03/12/2010	337	IT-Ro2	18/05/2011	138	IT-Ren	22/08/2011	234	IT-Col	30/09/2010	273
IT-Col	03/12/2010	337	IT-Lav	22/05/2012	143	IT-Col	22/08/2011	234	IT-Ro2	02/10/2010	275
IT-Ro2	10/12/2010	344	IT-Ro4	30/05/2012	151	IT-Col	28/08/2010	240	IT-Ren	14/10/2010	287
IT-Col	10/12/2010	344	IT-Lav	30/05/2012	151	IT-Ro2	28/08/2010	240	IT-Ro2	28/09/2011	271

Aiming to develop a new approach for actual ET assessment, Minacapilli et al. (2016) proposed and tested, in an Italian region (Sicily), a new method based on a combined and stand-alone use of MODIS and MSG-SEVIRI products able to estimate R_n and ET without the use of ancillary data (i.e. ground measurements).

The objective of this work was to evaluate the satellite stand-alone approach for deriving R_n, proposed by Minacapilli et al., (2016), over different climate/land-use sites and at different temporal resolution (daily and 8-day scale). The obtained R_n product, as well as its singular components, was validated using the radiation fluxes provided by 9 stations of FLUXNET network spread along Italy. A step-forward consists of testing the sensitivity of the algorithm in function of site-dependent parameters (ε_0, T_s, EVI, elevation) and their relations.

2. Materials and methods

2.1. R_n model description

The estimation of R_n (W m^{-2}) is obtained by summing up the net surface shortwave (R_{ns}) and longwave (R_{nl}) radiation, as follows:

$$R_n = R_{ns} + R_{nl} = R_{ss\downarrow} - R_{ss\uparrow} + R_{sl\downarrow} - R_{sl\uparrow} - (1-\varepsilon_0) \bullet R_{sl\downarrow} \quad (1)$$

where, $R_{ss\downarrow}$ is the incoming shortwave radiation emitted by the sun and transmitted through atmosphere (W m^{-2}); $R_{ss\uparrow}$ is the outgoing shortwave radiation (W m^{-2}) depending on $R_{ss\downarrow}$ and surface albedo (α); $R_{sl\downarrow}$ is the downward longwave radiation (W m^{-2}), $R_{sl\uparrow}$ is the upward longwave radiation (W m^{-2}), and ε_o is the surface thermal emissivity.

$R_{sl\uparrow}$ component is derived from the Stefan–Boltzmann equation, as follows:

$$R_{sl\uparrow} = \varepsilon_0 \bullet \sigma \bullet T_{s,avg}^4 \quad (2)$$

where, σ is the Stefan–Boltzmann constant (5.67×10^{-8} W m^{-2} K^{-4}), and $T_{s,\ avg}$ (K) is the diurnal-night-time mean T_s.

2.1.1. Remote sensing data input

The R_n algorithm, herein described, using a satellite-based stand-alone procedure, which exploits the potential of a set of time series products supplied by MODIS and MSG - SEVIRI sensors. Table 1 displays the satellite products used in this study and their main characteristics.

Daily and 8-day T_s, ε_o (MOD11 A1 and MOD11 A2, with a 1000 m resolution) and broadband α products (MCD43A3, with a 500 m resolution) were retrieved from the Land Processes Distributed Active

Table 5
Seasonal and all period statistical performances (BIAS, MAE, RMSE in W m^{-2} and R^2) of the daily average R_n modelled in respect to the selected Italian FLUXNET stations at the selected dates within the reference period 2010-12.

Reference period (2010–2012)	Equation	BIAS (W m^{-2})	MAE (W m^{-2})	RMSE (W m^{-2})	R^2
Winter (Dec - Feb)	y = 0.98x − 17.39	−17.5	26.3	33.8	0.45
Spring (Mar - May)	y = 0.97x − 0.01	−4.0	13.2	16.0	0.90
Summer (Jun - Aug)	y = 0.77x + 32.95	−0.7	15.2	21.2	0.58
Autumn (Sep - Nov)	y = 0.91x + 10.00	−7.1	15.7	18.3	0.75
All period	y = 1.04x − 11.53	−7.3	17.6	23.3	0.92

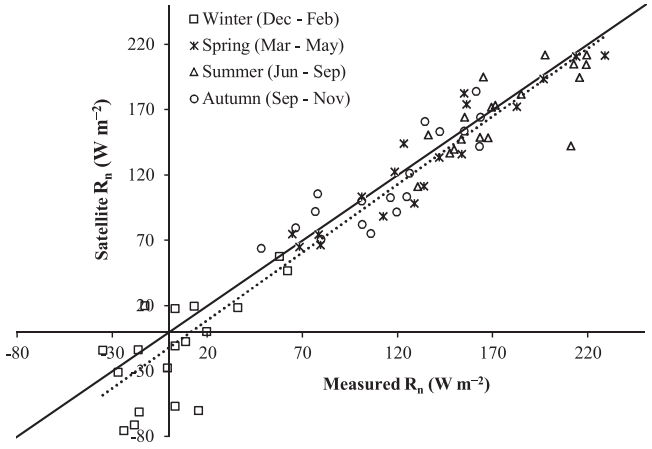

Fig. 2. Global comparison of daily average R_n (W m^{-2}) from satellite and FLUXNET measurements within the reference period at the following 4 seasons: Winter (Dec–Feb), Spring (Mar–May), Summer (Jun–Aug), and Autumn (Sep–Nov); the dashed and solid lines represent the regression line and the 1:1 line, respectively.

Archive Centre - LP DAAC (http://lpdaac.usgs.gov/). Both daytime and night-time products of T_s are required in order to calculate $T_{s,\ avg}$ (see Eq. (2)). Albedo (α) product was obtained using 16-day composite datasets from both Terra and Aqua satellites. The MODIS composite technique includes the determination of the two greatest α values for each pixel at the 16-day composite interval (Kim and Hogue, 2013).

SEVIRI sensor on-board MSG satellite includes 3 short-wave channels (0.6 μm, 0.8 μm, and 1.6 μm) with 15 min acquisition intervals. This enables to directly retrieve $R_{ss\downarrow}$ (DSSF product, Level 1.5 DIDSSF LSA-09) and $R_{sl\downarrow}$ (DSLF product, Level 1b DIDSLF LSA-12) radiation components from LSA-SAF (http://landsaf.meteo.pt). DSLF products were derived from a hybrid algorithm, which integrates cloud masks developed by the NWC-SAF (Nowcasting and Very Short-Range Forecasting, http://www.nwcsaf.org/, Derrien and Le Gléau, 2005) and forecasts on atmospheric profiles, rainfall and near surface air temperature, provided by the European Centre for Medium-range Weather Forecasts (ECMWF).

2.1.2. FLUXNET network

FLUXNET data were retrieved for validating R_n estimates derived from the proposed model. FLUXNET is a global network of micrometeorological tower sites that use eddy covariance (EC) method to measure the exchanges of mass and energy between terrestrial ecosystems and the atmosphere (https://fluxnet.ornl.gov/). Table 2 reports the FLUXNET data availability in the selected area, corresponding to Italy region (Fig. 1), within the reference period 2010-12. In Table 3 the details of the Italian FLUXNET demo-sites used in this study are reported. The EC measurement height varied from 2.5 m in grassland (IT-MBo in Tables 2 and 3; Marcolla et al. 2011) to more than 40 m in forests (IT-Lav and IT-Ren in Tables 2 and 3; Cescatti and Marcolla, 2014).

2.1.3. Daily average R_n and components

Daily satellite data input were selected (T_s, ε_o, α, $R_{ss\downarrow}$, and $R_{sl\downarrow}$) and estimated ($R_{ss\uparrow}$, $R_{sl\uparrow}$, by Eqs. (1) and (2)) for running the R_n model (Eq. (1)) at daily scale. Overall, 72 dataset were selected within the observation period 2010–2012, 18 dataset for each one of the following 4 seasonal periods: Winter (December–February), Spring (March–May), Summer (June–August), and Autumn (September–November). Data were selected on the basis of cloudless condition and are reported in Table 4. In order to select only clear sky days, two conditions were considered for both image selection and field data. First, cloud-free satellite imagery were chosen based on the criteria considered by Wan (2013). Secondly, for those days meet the previous condition, an exhaustive analysis was performed based on the hourly FLUXNET data (R_n values) selecting only days with a normal daily R_n pattern (it means, without peaks caused by the clouds).

2.1.4. 8-day average R_n and components

8-day T_s / ε_o, the combined 8-day time series of α and R_n components, allow the generation of 8-day average R_n. The number of selected MODIS Terra/Aqua overpasses was 114 during the observation period 2010–2012, between July and December. Daily R_n components, in particular $R_{ss\downarrow}$ and $R_{sl\downarrow}$, derived from LSA-SAF SEVIRI products, and $R_{ss\uparrow}$, $R_{sl\uparrow}$ estimated by Eqs. (1) and (2), were averaged at the 8-day timestep for homogeneity with the MODIS dataset.

Table 6
Site-to-site statistical performances (BIAS, MAE, RMSE in W m^{-2} and R^2) of the daily average R_n (W m^{-2}) from satellite and ground measurements for the selected dates within the reference period 2010-12.

Station	Equation	BIAS (W m^{-2})	MAE (W m^{-2})	RMSE (W m^{-2})	R^2
IT-Col	y = 0.96x − 4.42	−8.27	20.86	25.56	0.87
IT-Lav	y = 1.16x − 37.39	−19.60	20.63	28.24	0.98
IT-Ren	y = 0.92x + 9.59	1.25	11.51	14.16	0.97
IT-Ro2	y = 1.04x − 8.72	−3.50	14.45	16.85	0.94
IT-Ro4	y = 1.27x − 54.49	−31.51	35.69	45.27	0.94

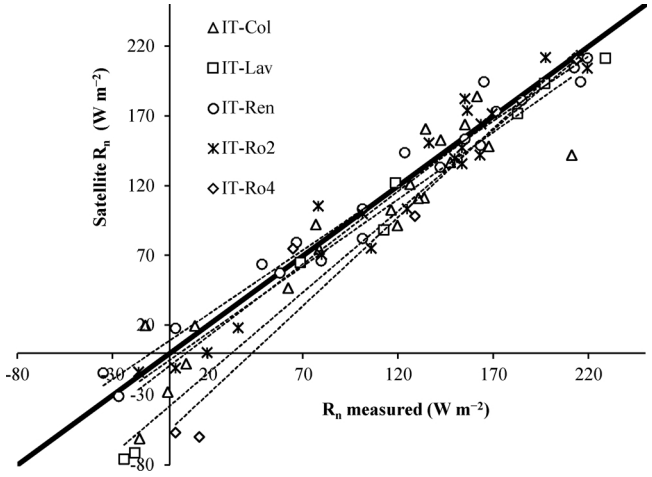

Fig. 3. Site-to-site comparison of daily average R_n (W m^{-2}) from satellite and ground measurements for the selected dates within the reference period 2010–12; the dashed and solid lines represent the regression lines and the 1:1 line, respectively.

2.2. R_n model performance

2.2.1. Statistical analyses

The intercomparison between ground and satellite-based R_n (and its components $R_{ss\downarrow}$, $R_{sl\downarrow}$, $R_{ss\uparrow}$, $R_{sl\uparrow}$) was assessed over the validation site using different statistical indices, including: mean bias error (BIAS); mean absolute difference (MAE); root mean square error (RMSE); and coefficient of determination (R^2).

2.2.2. Sensitivity analysis

A sensitivity analysis was performed in order to assess the impact of individual changes in α, ε_o and T_s on R_n estimation. In order to cover a wide range of model accuracies, 2 days, with different magnitude errors were selected: DOY 245 of 2010 at IT-Ro2 FLUXNET site (Table 2) with a low error in R_n estimation; and DOY 234 of 2011 at IT-Col FLUXNET site (Table 2) with a large error in R_n estimation. The procedure for assessing the individual effect of α and T_s consists of keeping constant all the variables, change the target variable between a range of values and evaluate how the R_n value is modified. However, for the specific case of ε_o sensitivity analysis, α was kept constant but T_s was corrected for each ε_o variation according to the relationship found by Ramírez-Cuesta et al. (2017b). α considered domain ranged from 0.05 to 0.30 in

Table 7
Statistical performances (BIAS, MAE, RMSE in W m^{-2} and R^2) of the daily average R_n components ($R_{ss\downarrow}$, $R_{sl\downarrow}$, $R_{ss\uparrow}$, $R_{sl\uparrow}$) retrieved / estimated by satellite at the selected Italian FLUXNET stations for the selected dates within the reference period 2010–12.

R_n Components	Equation	BIAS (W m^{-2})	MAE (W m^{-2})	RMSE (W m^{-2})	R^2
$R_{ss\downarrow}$	y = 1.00x − 4.78	−4.3	35.0	33.0	0.87
$R_{sl\downarrow}$	y = 0.80x + 82.06	25.5	31.0	39.5	0.63
$R_{ss\uparrow}$	y = 0.98x + 2.70	2.3	6.5	8.9	0.67
$R_{sl\uparrow}$	y = 1.30x − 83.73	21.0	23.0	33.4	0.78

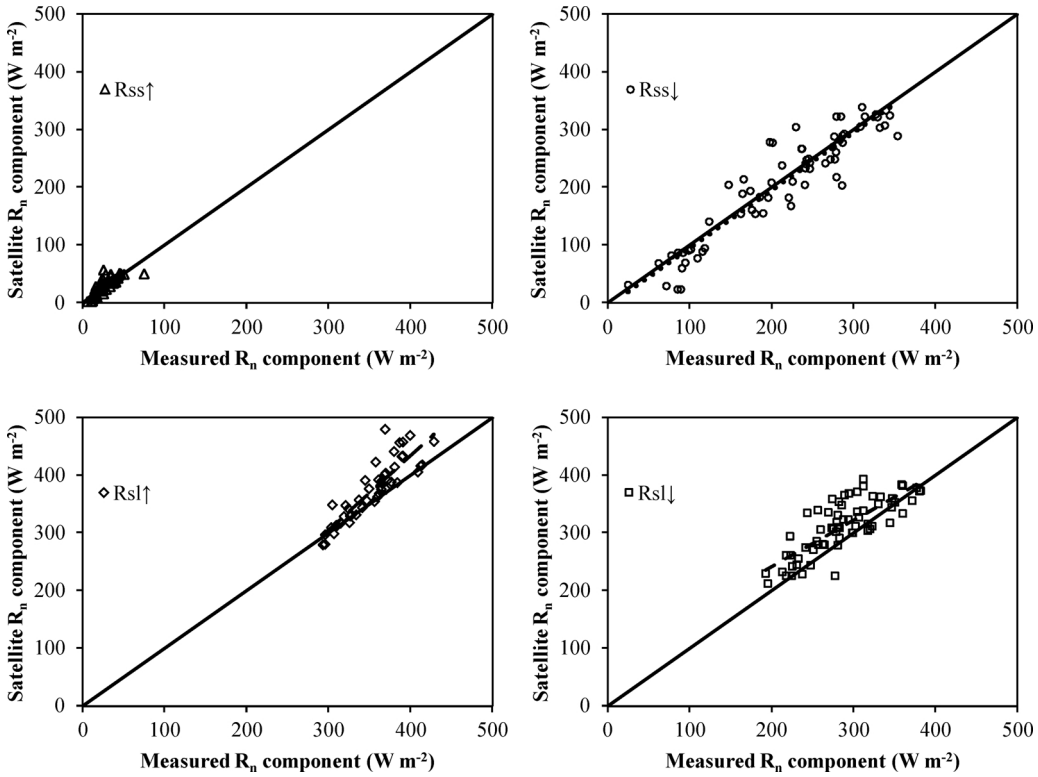

Fig. 4. Global comparison of daily average R_n components ($R_{ss\downarrow}$, $R_{sl\downarrow}$, $R_{ss\uparrow}$, $R_{sl\uparrow}$, in W m^{-2}) from satellite and ground measurements for the selected dates within the reference period 2010–12; the dashed and solid lines represent the regression lines and the 1:1 line, respectively.

Table 8
Site-to-site statistical performances (BIAS, MAE, RMSE in W m^{-2} and R^2) of the daily average R_n components ($R_{ss\downarrow}$, $R_{sl\downarrow}$, $R_{ss\uparrow}$, $R_{sl\uparrow}$, W m^{-2}) from satellite and ground measurements for the selected dates within the reference period 2010-12.

		$R_{ss\downarrow}$	$R_{sl\downarrow}$	$R_{ss\uparrow}$	$R_{sl\uparrow}$
IT-Col	BIAS (W m^{-2})	5.7	49.2	6.5	47.0
	MAE (W m^{-2})	31.7	54.2	8.1	47.0
	RMSE (W m^{-2})	39.2	57.8	10.6	55.7
	R^2	0.80	0.50	0.77	0.85
IT-Lav	BIAS (W m^{-2})	−23.2	6.8	3.4	5.2
	MAE (W m^{-2})	25.7	17.9	7.2	7.2
	RMSE (W m^{-2})	34.1	21.4	12.3	10.1
	R^2	0.98	0.96	0.78	0.90
IT-Ren	BIAS (W m^{-2})	−13.2	25.1	2.9	9.2
	MAE (W m^{-2})	26.2	26.1	6.1	12.9
	RMSE (W m^{-2})	30.1	31.8	7.1	16.6
	R^2	0.86	0.81	0.63	0.91
IT-Ro2	BIAS (W m^{-2})	1.8	5.6	−2.0	22.9
	MAE (W m^{-2})	15.9	17.7	5.3	24.2
	RMSE (W m^{-2})	22.7	27.3	7.3	29.7
	R^2	0.94	0.55	0.79	0.85

steps of 0.01; ε_o varied from 0.95 to 1.00 in 0.0025 steps; and T_s domain was defined as ± 15 K of the daily temperature in steps of 1 K.

3. Results

This section is divided into three subsections. The first one is focused on the evaluation of the R_n estimates by the proposed model (and its components) with respect to the radiation fluxes measured at the selected Italian FLUXNET demo-sites both at daily and 8-day temporal scale. Second, the results of the sensitivity analysis of the main parameters involved in R_n estimation are reported. Finally, in the third subsection, some examples of final outputs retrieved by the model are showed.

3.1. Comparison between measured and modelled R_n and components

This subsection presents the main results, in terms of statistical performances, of the intercomparison between ground measurements and satellite-based R_n estimates (and its components $R_{ss\downarrow}$, $R_{sl\downarrow}$, $R_{ss\uparrow}$, $R_{sl\uparrow}$) at each selected demo-site (Table 2 and Fig. 1), within the observation period 2010–2012 both at daily and 8-day temporal scale.

3.1.1. Daily average R_n and components

Table 5 shows the statistical metrics (BIAS, MAE, RMSE in W m^{-2} and R^2) of the daily average R_n estimated by the proposed model at the demo-sites. Results are displayed in 4 seasonal clusters referring to the selected dates within the reference period 2010–12 as reported in Table 4.

At daily scale, the average R_n estimates showed a fairly good agreement with the measured R_n at the selected Italian FLUXNET stations. The overall BIAS, MAE and RMSE were −7.3, 17.6 and 23.3 W m^{-2} respectively, with an R^2 of 0.92 (Table 5). Based on the seasonality (Table 5), it can be observed that the highest BIAS, MAE and RMSE (−17.5, 26.3 and 33.8 W m^{-2}, respectively) and lowest R^2 (0.45) are obtained in Winter. The behaviour observed in the other seasons (Spring, Summer and Autumn) is quite similar, with values ranging from −0.7 to −7.1 W m^{-2} for BIAS, from 13.2 to 15.7 W m^{-2} for MAE, from 16.0 to 21.2 W m^{-2} for RMSE, and from 0.58 to 0.90 for R^2.

Fig. 2 displays the scatter-plot of the ground R_n measurements and satellite-based R_n estimates (W m^{-2}) at the selected Italian FLUXNET sites within the considered 4 seasonal periods in 2010–12.

Table 6 and Fig. 3 report the details of site-to-site statistical performances (BIAS, MAE, RMSE in W m^{-2} and R^2) and the comparison of the daily average R_n (W m^{-2}) from satellite and ground measurements for the selected dates within the reference period 2010–12, respectively.

No large discrepancies were observed at the site-to-site daily average R_n comparisons: with absolute BIAS, MAE and RMSE values less than 31.5, 35.7 and 45.3 W m^{-2}, respectively, at all sites, and R^2

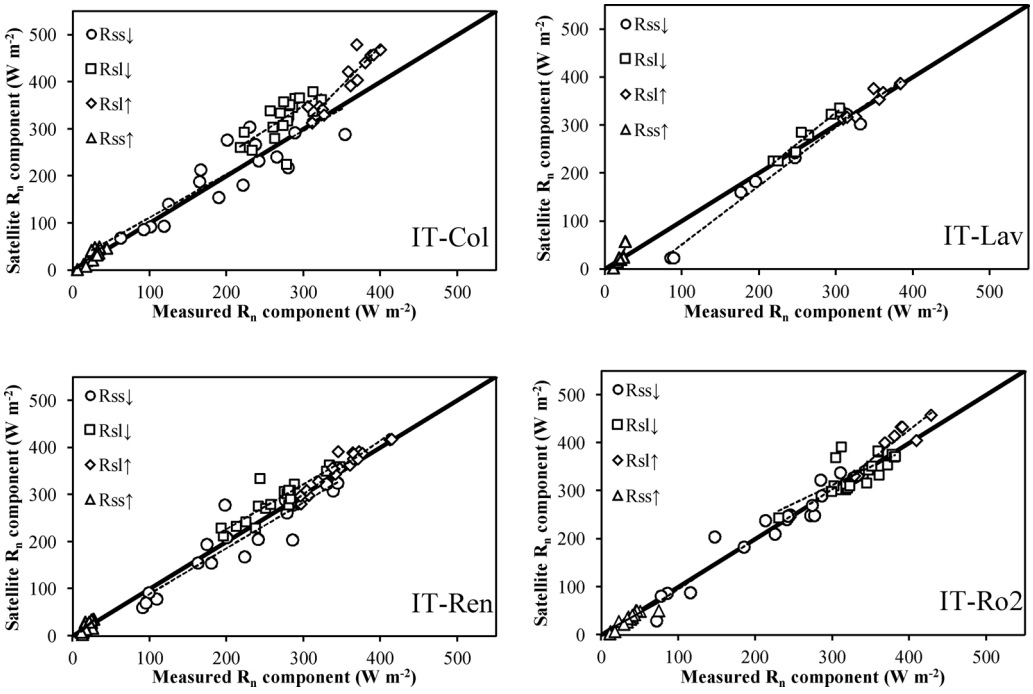

Fig. 5. Site-to-site comparisons of daily average R_n components ($R_{ss\downarrow}$, $R_{sl\downarrow}$, $R_{ss\uparrow}$, $R_{sl\uparrow}$, W m^{-2}) from satellite and ground measurements for the selected dates within the reference period 2010–12; the dashed and solid lines represent the regression lines and the 1:1 line, respectively.

Table 9
Statistical performances (BIAS, MAE, RMSE in W m^{-2} and R^2) of the 8-day R_n estimated by the proposed model at the selected Italian FLUXNET stations in 2010–12.

Station	Year	Equation	BIAS (W m^{-2})	MAE (W m^{-2})	RMSE (W m^{-2})	R^2
IT-CA1	2012	y = 1.07x − 36.51	−28.8	29.0	34.8	0.89
IT-CA2	2012	y = 0.99x − 16.45	−12.3	17.9	21.9	0.89
IT-CA3	2012	y = 0.96x + 0.81	−3.1	15.4	20.4	0.88
IT-Col	2010	y = 1.01x − 21.09	−20.6	24.8	27.6	0.91
	2011	y = 0.92x − 6.96	−15.5	16.4	19.1	0.98
	2012	y = 1.05x − 30.28	−23.8	24.1	30.9	0.92
IT-Lav	2010	y = 0.99x − 5.39	−6.5	16.6	20.1	0.92
	2011	y = 0.99x − 0.05	−1.5	8.0	10.1	0.98
	2012	y = 1.01x − 8.21	−7.5	12.6	16.9	0.96
IT-MBo	2010	y = 1.16x + 8.12	18.1	18.7	26.5	0.94
	2011	y = 1.00x + 27.52	27.7	28.2	32.9	0.94
	2012	y = 0.97x + 16.66	15.2	20.5	24.9	0.92
IT-Ren	2010	y = 0.95x − 14.00	−17.7	20.2	23.2	0.96
	2011	y = 1.02x − 19.09	−17.5	18.6	21.8	0.97
IT-Ro2	2010	y = 0.88x − 8.09	−19.2	19.2	24.1	0.97
	2011	y = 0.88x + 37.18	29.9	30.8	37.3	0.90
IT-Ro4	2012	y = 1.07x − 10.05	−3.2	13.4	18.3	0.92
All stations	2010	y = 0.95x − 5.89	−9.8	19.6	24.0	0.90
	2011	y = 0.91x + 13.16	6.1	21.2	27.0	0.88
	2012	y = 0.95x − 4.46	−7.7	18.7	24.5	0.88
All stations	2010–12	y = 0.93x + 2.04	−3.1	19.8	25.4	0.87

values ranged from 0.87 to 0.98. Despite the general good agreement, lower performances were observed at certain sites as IT-Lav and IT-Ro4, with trend lines slopes higher than 1.15 and the highest absolute BIAS, MAE and RMSE values among all sites (Table 6).

Table 7 reports the statistical metrics of the daily average R_n single components ($R_{ss\downarrow}$, $R_{sl\downarrow}$, $R_{ss\uparrow}$, $R_{sl\uparrow}$) retrieved by LSA-SAF SEVIRI ($R_{ss\downarrow}$, $R_{sl\downarrow}$) and estimated in this study ($R_{ss\uparrow}$, $R_{sl\uparrow}$, by Eqs. (1) and (2)) compared to the observed daily values recorded at the selected Italian

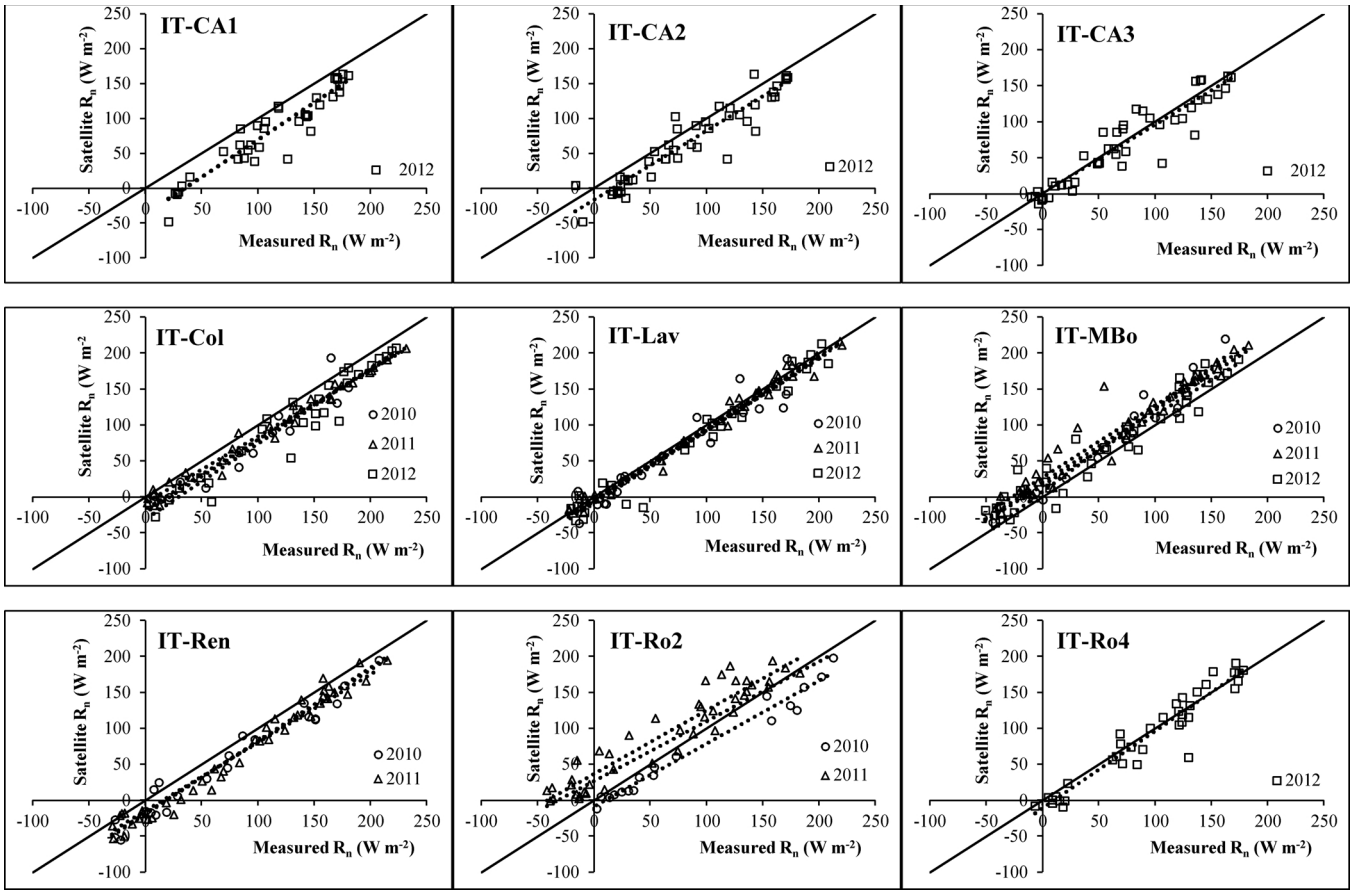

Fig. 6. (previous page) Site-to-site comparisons of 8-day average R_n (W m^{-2}) from satellite and ground measurements within the reference period 2010–12 for each one of the selected Italian FLUXNET site; the dashed and solid lines represent the regression lines and the 1:1 line, respectively.

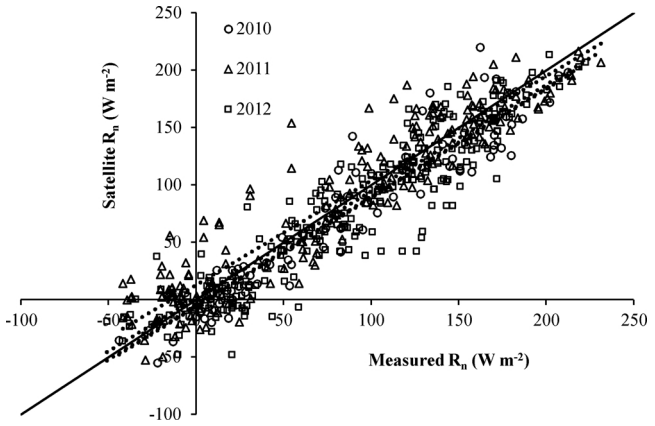

Fig. 7. Global comparison of 8-day average R_n estimates (W m^{-2}) from satellite and ground measurements during the 3 years of the reference period; the dashed and solid lines represent the regression lines and the 1:1 line, respectively.

FLUXNET stations for the selected dates of 2010-12 period (Table 4). In general, the R_n single components estimates showed an excellent agreement with ground measured components at the selected demo-sites. However, estimates of shortwave components ($R_{ss\downarrow}$ and $R_{ss\uparrow}$) were much more accurate than longwave components ($R_{sl\downarrow}$ and $R_{sl\uparrow}$). Shortwave components showed lower absolute values of BIAS (− 4.3 – 2.3 W m^{-2} for shortwave components *versus* 21.0–25.5 W m^{-2} for longwave components) and better fits with the 1:1 line (slope terms of 0.98–1.00 for shortwave components *versus* slope terms of 0.80–1.30 for longwave components) than longwave components (Table 7 and Fig. 4).

Fig. 4 shows the relationship between the daily average R_n components ($R_{ss\downarrow}$, $R_{sl\downarrow}$, $R_{ss\uparrow}$, $R_{sl\uparrow}$, in W m^{-2}) obtained from satellite (retrieved or estimated) and the R_n components recorded at the Italian FLUXNET stations for the selected dates within the reference period 2010–12.

Table 8 and Fig. 5 report the details of the site-to-site statistical performances (BIAS, MAE, RMSE in W m^{-2} and R^2) and the comparisons of the daily average R_n components ($R_{ss\downarrow}$, $R_{sl\downarrow}$, $R_{ss\uparrow}$, $R_{sl\uparrow}$, W m^{-2})

Table 10
Statistical performances (BIAS, MAE, RMSE in W m^{-2} and R^2) of the 8-day average R_n components ($R_{ss\downarrow}$, $R_{sl\downarrow}$, $R_{ss\uparrow}$, $R_{sl\uparrow}$) retrieved / estimated by satellite at the selected Italian FLUXNET stations within the reference period 2010–12.

R_n Components	Equation	BIAS (W m^{-2})	MAE (W m^{-2})	RMSE (W m^{-2})	R^2
$R_{ss\downarrow}$	y = 0.97x − 2.08	−7.5	23.0	30.8	0.88
$R_{sl\downarrow}$	y = 0.78x + 66.27	2.3	22.0	27.9	0.65
$R_{ss\uparrow}$	y = 0.32x + 9.54	−9.4	11.5	20.9	0.35
$R_{sl\uparrow}$	y = 1.17x − 36.82	25.6	28.0	34.8	0.85

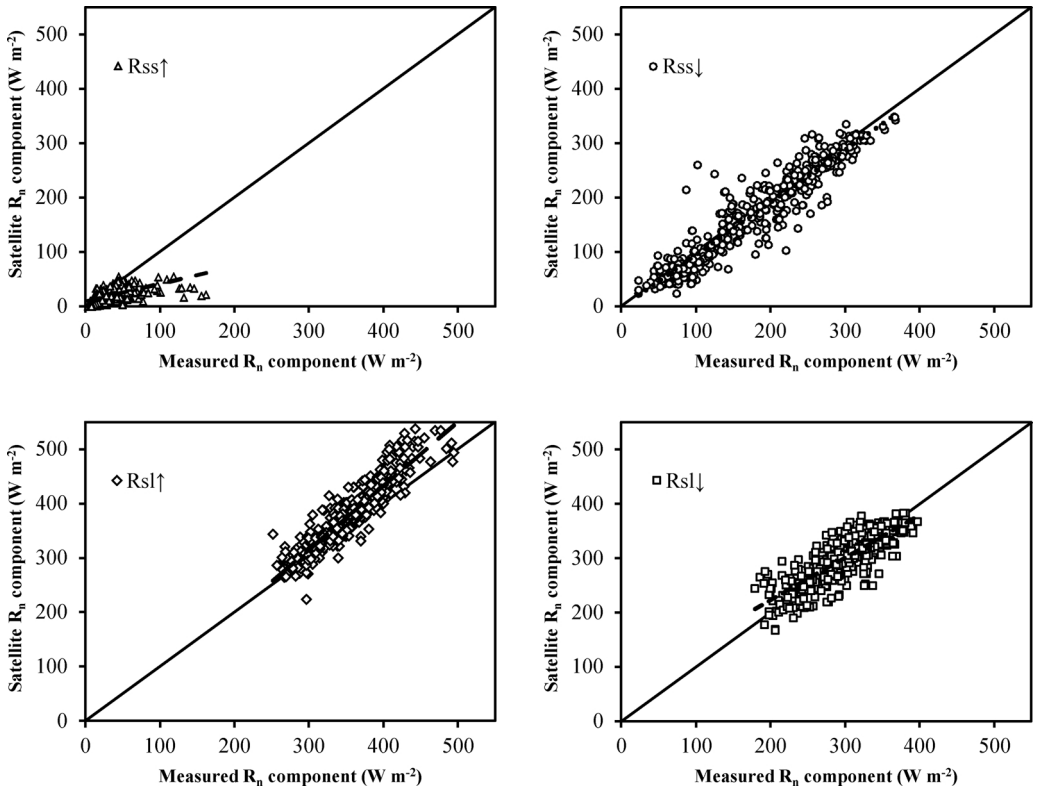

Fig. 8. Global comparison of 8-day average R_n components ($R_{ss\downarrow}$, $R_{sl\downarrow}$, $R_{ss\uparrow}$, $R_{sl\uparrow}$, in W m^{-2}) from satellite and ground measurements for all demo-sites within the reference period 2010–12; the dashed and solid lines represent the regression lines and the 1:1 line, respectively.

Table 11
Statistical performances (BIAS, MAE, RMSE in W m^{-2} and R^2) of the 8-day average R_n components ($R_{ss\downarrow}$, $R_{sl\downarrow}$, $R_{ss\uparrow}$, $R_{sl\uparrow}$, W m^{-2}) from satellite and ground measurements at the selected Italian FLUXNET stations in 2010–12.

Station	Statistics	$R_{ss\downarrow}$	$R_{sl\downarrow}$	$R_{ss\uparrow}$	$R_{sl\uparrow}$
IT-CA1	BIAS (W m^{-2})	−5.9	−19.2	−6.6	27.1
	MAE (W m^{-2})	33.2	25.2	8.7	30.4
	RMSE (W m^{-2})	40.2	30.9	10.6	39.7
	R^2	0.73	0.55	0.64	0.80
IT-CA2	BIAS (W m^{-2})	−5.5	−24.7	−10.5	28.1
	MAE (W m^{-2})	30.5	27.1	10.6	31.5
	RMSE (W m^{-2})	36.0	32.0	14.1	39.4
	R^2	0.80	0.71	0.66	0.76
IT-CA3	BIAS (W m^{-2})	1.8	−21.0	−3.3	28.0
	MAE (W m^{-2})	30.9	27.4	6.1	27.5
	RMSE (W m^{-2})	38.8	34.0	7.7	35.7
	R^2	0.69	0.45	0.67	0.74
IT-Col	BIAS (W m^{-2})	−17.9	30.3	−2.6	39.8
	MAE (W m^{-2})	19.2	24.5	3.9	39.8
	RMSE (W m^{-2})	24.5	27.0	5.3	42.2
	R^2	0.96	0.87	0.95	0.92
IT-Lav	BIAS (W m^{-2})	−5.7	15.3	−2.2	18.2
	MAE (W m^{-2})	11.4	15.8	4.5	19.1
	RMSE (W m^{-2})	15.6	18.8	5.4	22.6
	R^2	0.97	0.91	0.86	0.94
IT-MBo	BIAS (W m^{-2})	−7.9	27.6	−35.1	26.3
	MAE (W m^{-2})	31.2	31.8	35.5	29.3
	RMSE (W m^{-2})	40.8	37.6	44.8	35.3
	R^2	0.77	0.67	0.23	0.79
IT-Ren	BIAS (W m^{-2})	−9.1	6.5	1.2	15.6
	MAE (W m^{-2})	15.4	12.3	3.6	19.6
	RMSE (W m^{-2})	17.9	17.7	4.7	23.2
	R^2	0.97	0.89	0.67	0.92
IT-Ro2	BIAS (W m^{-2})	−0.7	7.6	−4.9	54.4
	MAE (W m^{-2})	14.9	9.8	6.8	52.6
	RMSE (W m^{-2})	18.0	10.6	7.4	59.7
	R^2	0.98	0.91	0.96	0.96
2010	BIAS (W m^{-2})	−12.7	−1.0	−7.4	19.2
	MAE (W m^{-2})	23.2	16.9	9.0	26.0
	RMSE (W m^{-2})	29.6	22.3	12.6	35.0
	R^2	0.91	0.76	0.56	0.86
2011	BIAS (W m^{-2})	−3.6	5.2	−10.4	26.4
	MAE (W m^{-2})	19.1	21.2	11.9	27.1
	RMSE (W m^{-2})	25.9	26.4	22.7	32.8
	R^2	0.91	0.68	0.42	0.88
2012	BIAS (W m^{-2})	−9.0	0.8	−9.2	27.5
	MAE (W m^{-2})	26.5	25.1	12.1	29.2
	RMSE (W m^{-2})	35.2	31.3	22.0	35.8
	R^2	0.84	0.59	0.25	0.83

from satellite and ground measurements for the selected dates within the reference period 2010–12, respectively.

3.1.2. 8-day average R_n and components

Table 9 shows the statistical metrics (BIAS, MAE, RMSE in W m^{-2}, and R^2) of the 8-day average R_n estimated by the proposed model (Eq. (1)) at the selected demo-sites in 2010–12 period (Table 2 and Fig. 1).

The overall performance statistics (all reference period) show a BIAS, RMSE and MAE of −3.1, 19.8 and 25.4 W m^{-2}, respectively and an R^2 of 0.87 (Table 9 and Fig. 6). In particular, the performance statistics (BIAS, MAE, RMSE) in 2010 were −9.8, 19.6, 24.0 W m^{-2} with R^2 of 0.90; in 2011, were 6.1, 21.2, 27.0 W m^{-2} with R^2 of 0.88; and in 2012 were −7.7, 18.7, 24.5 W m^{-2}, and 0.88, respectively (Table 9 and Fig. 6).

Regarding site-to-site differences, no large discrepancies among the selected demo-sites were observed. Thus, absolute BIAS, MAE and RMSE values were less than 30, 31 and 38 W m^{-2}, respectively, at all sites. In addition, R^2 values ranged from 0.88 to 0.98, highlighting the good agreement between R_n derived from remote sensing and the measured at the selected demo-sites.

Figs. 6 and 7 show the comparison between observed and satellite-based R_n estimates (W m^{-2}) in respect to the 3 years of study (2010, 2011, and 2012), at the single selected FLUXNET Italian site (Table 2), and for the overall sites together, respectively. It can be observed that the trend lines for each specific site (Fig. 6) and considering all sites together (Fig. 7) show a good agreement among the different years in all cases except for IT-Ro2. Thus, the performance of the proposed model is, in general, quite constant for all years.

Table 10 reports the statistical metrics of the 8-day average observed / modelled R_n single components ($R_{ss\downarrow}$, $R_{sl\downarrow}$, $R_{ss\uparrow}$, $R_{sl\uparrow}$) at the selected Italian FLUXNET stations for the 2010–12 period (Table 4). As for the daily R_n single components comparison, the estimates showed an excellent agreement with measured components at the selected demo-sites, except for the R^2 of $R_{ss\uparrow}$ component (Fig. 8).

Looking at the demo-site scale, this behaviour may be explained by the lowest fit, between provided / estimated and modelled R_n components, observed at IT-MBo station (Table 11). In this Table, the statistical performances are reported for each selected demo-site. In particular, the best performances, in terms of smallest BIAS values, for the R_n single components were observed as follows: for $R_{ss\downarrow}$ (−0.7 W m^{-2}) at IT-Ro2 site; and for $R_{sl\downarrow}$ (6.5 W m^{-2}), $R_{ss\uparrow}$ (1.2 W m^{-2}) and $R_{sl\uparrow}$ (15.6 W m^{-2}) at IT-Ren site.

Fig. 9 shows the site-to-site relationship between the 8-day average R_n components ($R_{ss\downarrow}$, $R_{sl\downarrow}$, $R_{ss\uparrow}$, $R_{sl\uparrow}$, W m^{-2}) obtained from satellite (retrieved or estimated) and the R_n components recorded at the Italian FLUXNET stations for the selected dates within the reference period 2010–12.

3.2. Sensitivity analysis

From the sensitivity analysis described in Section 2.2.2, the weight of α, ε_0 and T_s on R_n computation was assessed. Regarding α, each 0.01 variation in the α value (Δα) induced a linear R_n variation (ΔR_n) of 2.49 and 2.93 W m^{-2} for DOY 245 of 2010 and DOY 234 of 2011, respectively (Fig. 10a). When ε_0 effect on R_n calculation was assessed, a linear oscillation in R_n of 0.57–1.20 W m^{-2} per each 0.01 variation in the ε_0 ($\Delta\varepsilon_0$) value was observed (Fig. 10b). A R_n variation ranging from 5.87 to 6.24 W m^{-2} for DOY 245 (2010) and 234 (2011), respectively, was observed for each 1 K deviation in T_s (ΔT_s; Fig. 10c). However, contrary to the observed with the previous variables, ΔT_s – ΔR_n trend is not linear, but it fits a 4th degree curve.

3.3. R_n maps of Italy region

Fig. 11 shows an example of final output obtained from the proposed approach at 8-day scale. Particularly, for a geographical area including Italy, a set of 8-days R_n maps are represented for different seasonal period. As can be observed, the general variability of computed values across the four displayed periods resulted reliable, with typical highest values of R_n from June (Fig. 11b) to August (Fig. 11c) and lowest values in March (Fig. 11a) and October (Fig. 11d). The same example also shows how the output of model resulted able to capture the spatial patterns of R_n due to the mixture of different geographical attributes such as *α*, land cover/use, surface temperature, latitude and elevation.

With reference to the summer period of 2012 (August 4th–11th) Fig. 12(a–b) shows the net shortwave and net longwave components of R_n obtained by the proposed model. Also, in this case the variability of computed spatial patterns can be linked to the heterogeneity of surface

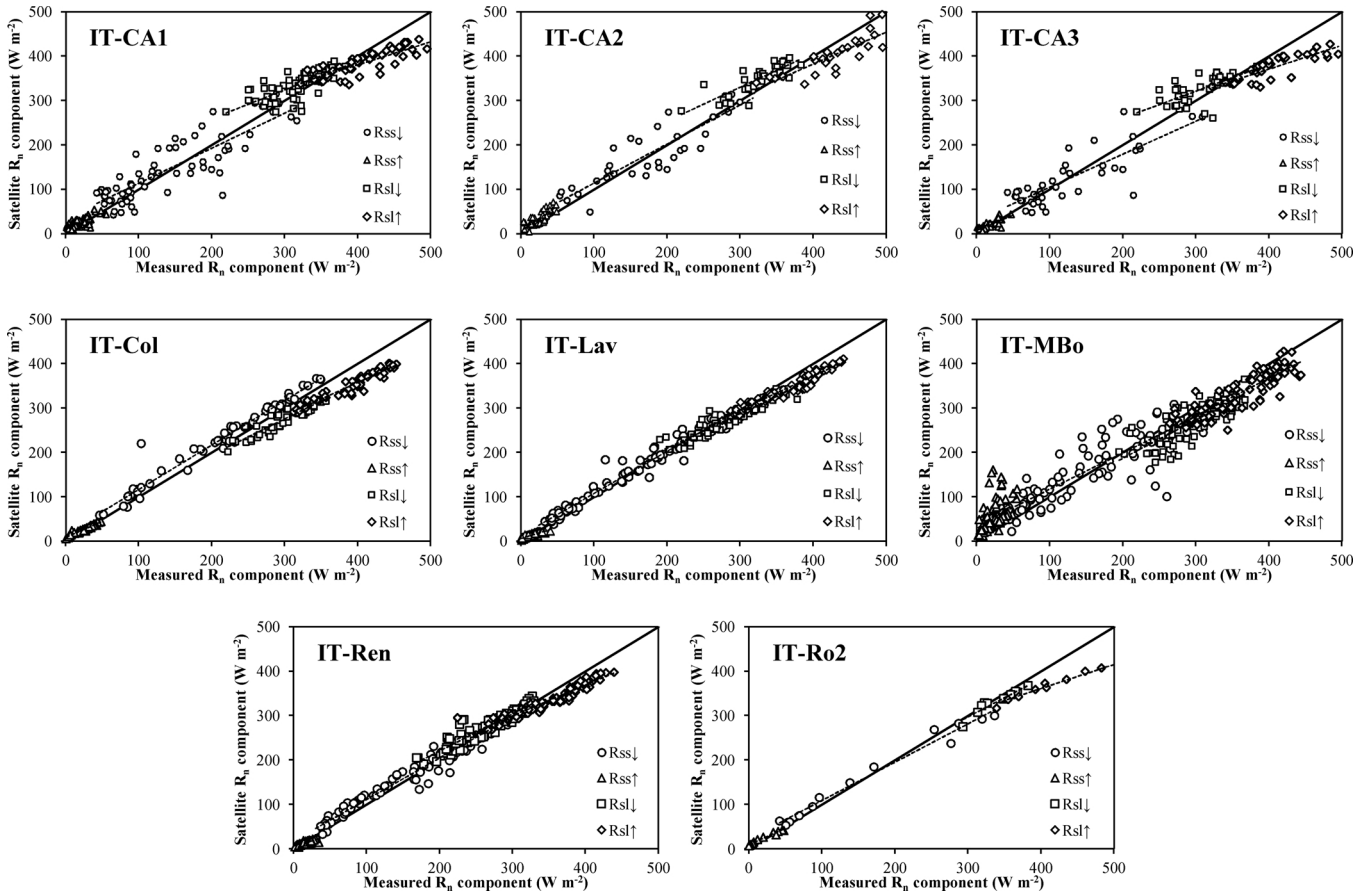

Fig. 9. (previous page) Site-to-site comparisons of 8-day average R_n components ($R_{ss\downarrow}$, $R_{sl\downarrow}$, $R_{ss\uparrow}$, $R_{sl\uparrow}$, W m^{-2}) from satellite and ground measurements within the reference period 2010–12 for each one of the selected Italian FLUXNET station; the dashed and solid lines represent the regression lines and the 1:1 line, respectively.

attributes. Particularly, as deduced by the results of sensitivity analysis, the density scatterplots showed in Fig. 12c and d highlight that the variability of surface α and T_s can be considered as main factor governing R_n respectively in short and longwave spectral domains.

4. Discussion

The proposed model has provided accurate estimates of R_n both at daily and 8-day time scale, with a RMSE and a MAE of 23.3 and 17.6 Wm^{-2} for daily scale; whereas these values were of 25.4 and 19.8 Wm^{-2} for a 8-day scale. Similar accuracies have been obtained by other authors under clear sky conditions (Bisht et al., 2005; Geiger et al., 2008; Journee and Bertrand, 2010; Hou et al., 2014; Gómez et al., 2016). In view of the results, no large differences among the different temporal scales in terms of accuracies were observed both in R_n and in the individual radiation components estimation, probably due to the proximity of both temporal scales. Several authors has observed errors compensation when more differentiated time scales are used (Geiger et al., 2008; Zhao et al., 2013; Gómez et al., 2016).

When results were assessed in term of the different seasons of the year, it was observed that in Winter, errors in R_n estimates were larger than in the other season of the year. Ramírez-Cuesta et al. (2017a) pointed out that a higher spatial heterogeneity of weather conditions is observed in Winter as unstable atmospheric conditions do not usually occur at the same time throughout wide regions. It implies that variables used in R_n estimation from remote sensing (as α, ε_0 and T_s) can vary from those measured at the demo-sites, since their footprints have different sizes. Cruz-Blanco et al. (2014) and Mardikis et al. (2005) also found this seasonal trend when evaluating reference ET assessment in Spain and Greece, respectively. However, this seasonal trend has a minimal impact on irrigation scheduling, since in semiarid climate conditions, the irrigation is mainly concentrated during Spring and Summer (Ramírez-Cuesta et al., 2017a). In respect to our results, R^2 is better for the overall period than for the specific seasons at daily scale because of compensation effects considering a wider range of values with a predominance of clear sky condition (Alados et al., 2003).

The site-to-site performance is quite dependent on the location characteristics (crop type, slope, and elevation, among others) and weather conditions (temperature and precipitation). Thus, the heterogeneity due to the alternation of croplands and bare soil in the area surrounding IT-Ro4 may be the main reason for the lower performance obtained for this site. However, discrepancies observed at IT-Lav were not due to heterogeneity but to the sloping terrain surrounding the tower, so the inherent assumption of horizontal terrain location of EC tower is not fulfilled. The presence of snow on the surface - mainly in the sites located at high elevations - also affects the Earth's energy balance, since it increases the amount of sunlight reflected by the ground and diminishes its temperature (Harding et al., 1995; Key et al., 1997), Thus, in those sites located at high elevations/latitudes (IT-Col, IT-Lav, IT-MBo and IT-Ren), special attention must be paid to the snow, since the results can be drastically affected by this phenomenon.

The performance of the proposed model is quite constant for all

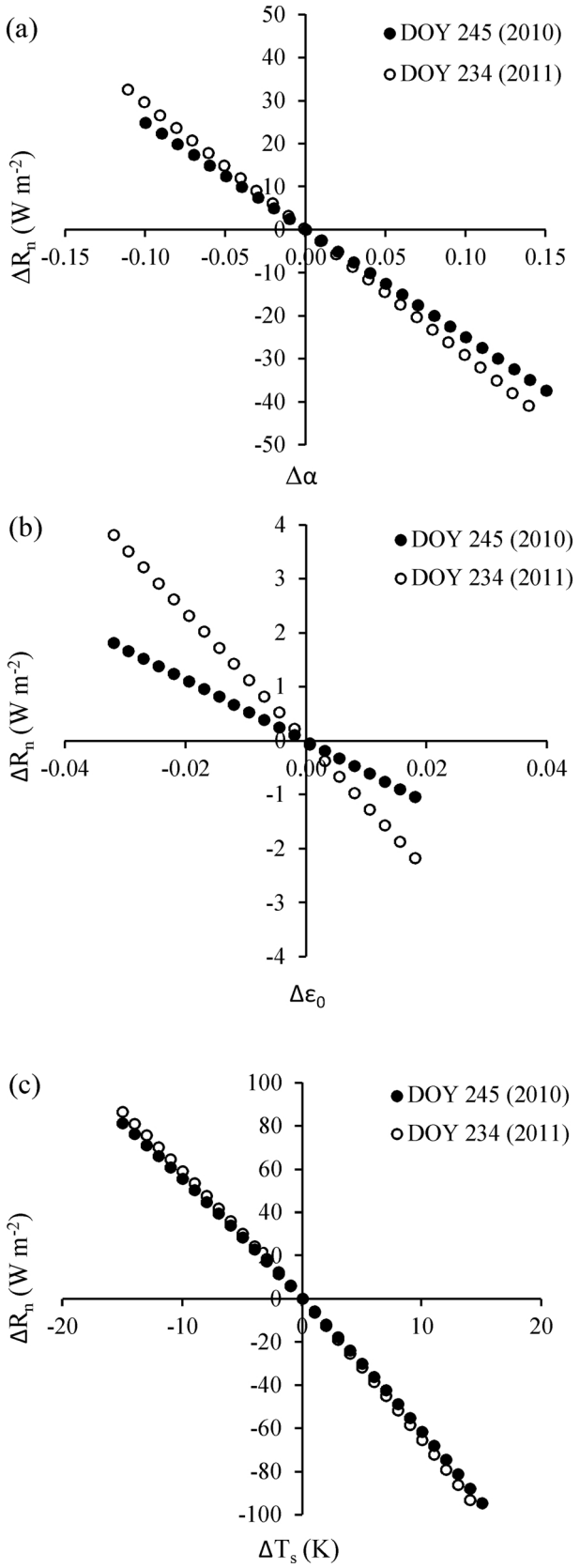

Fig. 10. Sensitivity analysis of α (a), ε_0 (b), and T_s (c) on R_n estimation.

years, although some temporal discrepancies were observed in IT-Ro2. Several reasons can explain the pattern observed in this site, such as malfunctions of the net radiometer, changes of sensor or need of calibration, for instance.

Regarding accuracies obtained for the different radiation components, statistical descriptors show that, generally, shortwave components provided better accuracies than longwave components (both downwelling and upwelling), the last being overestimated at both time scales. Contrary, shortwave components exhibited a slight underestimation. These over- and underestimation tendencies are related to the parameters involved in the estimation of the radiation components. The good results obtained for shortwave components means that (1) $R_{ss\downarrow}$ is not severely affected by the spatial scale discrepancies between satellite estimates and ground measurements; and (2) α values provided by MCD43A3 faithfully reflected the real α. On the other hand, estimated longwave components had more discrepancies when compared to the ground measurements. However, the reasons of such discrepancies vary depending on whether the component is downwelling or upwelling. Thus, Hou et al. (2014) pointed out that $R_{sl\downarrow}$ discrepancies are related to the difficult to acquire high spatial and temporal resolution information for air temperature and atmospheric emissivity, and to the elevation and topography components. These authors also found a slight overestimation, suggesting that it was probably caused by a overestimation of atmospheric emissivity. Moreover, it is important to consider that the DIDSLF-LAF $R_{sl\downarrow}$ product used in our model has been derived from an hybrid algorithm that assimilates global observations of atmospheric profiles and air temperatures to derive atmospheric emissivity under all sky conditions whose less or more accuracy directly affects $R_{sl\downarrow}$.

However, $R_{sl\uparrow}$ depends on T_s and ε_0. Hou et al. (2014) suggested that T_s discrepancies were possibly due to the heterogeneity of the land cover/use observing that densely vegetated sites during the growing season had a relatively smaller RMSE for the T_s than sparsely vegetated sites. These authors also pointed the fact that daytime T_s in MOD11 L2 product could not truly represent the T_s. Regarding ε_0, others authors has highlighted that its influence on R_n can be ignored when comparing with α and T_s influence (Zhou et al., 2010). It has been also observed in the sensitivity analysis performed in this study, highlighting that T_s plays an essential role in R_n estimation and that errors in α and ε_0 estimations results in low R_n errors.

Several authors have used micrometeorological techniques for validating energy balance fluxes obtained from satellite, pointing out the limitations regarding the mismatching between the footprint of field measurements and the pixel size of the satellite imagery (e.g. Bastiaanssen et al., 1998; Brunsell et al., 2011; Consoli et al., 2016; Consoli and Vanella, 2014; Tang et al., 2011). These limitations can cause large errors especially in heterogeneous locations with frequent land use transitions. The size of the footprint increases with an increase of the tower height and of the thermal stability; and with a decrease in the surface roughness. Nevertheless, the flux footprint around the towers considered in this study (varying from hundreds to few kilometers; Gockede et al., 2004), together with the relative homogeneity inside the pixels where the towers are placed, suggest that generally the results are not severely influenced by the mismatching phenomenon, altough it can explain specific errors observed in certain locations (as IT-Ro4 and IT-Lav).

Also looking at the output maps retrieved by the procedure (Figs. 11 and 12) and able to capture the spatial and temporal variability of R_n and its component it is clearly highlighted the roles of α and T_s variability in R_n estimation, as well as its components. The above surface parameters intrinsically varies with the mixture of land cover/use, latitude, elevation and anthropization and their effects on R_n that can be

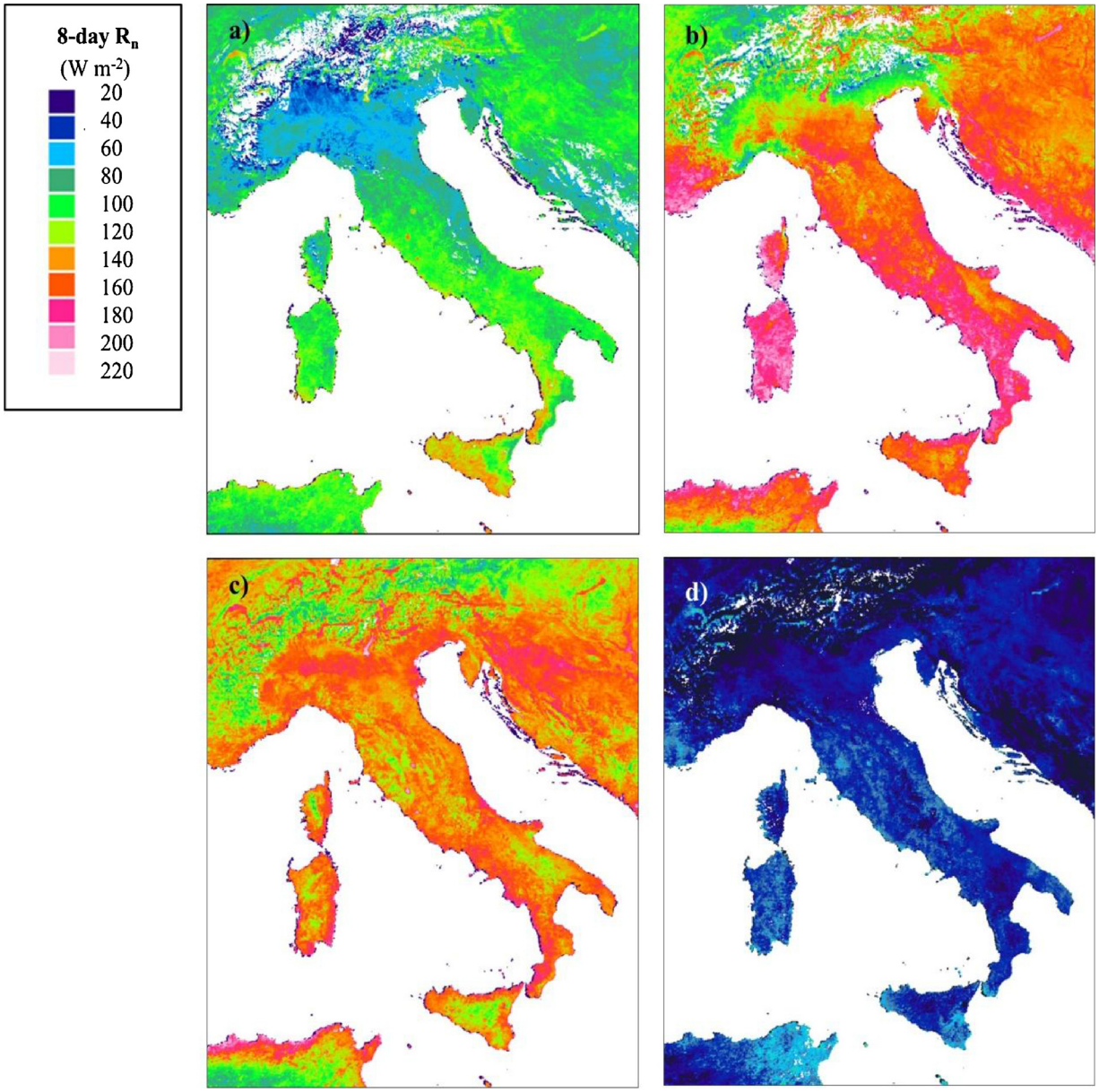

Fig. 11. R_n maps of Italy at 8-day scale, referring to March (a), June (b), August (c) and October (d), 2011.

easily assessed using the output maps that the procedure is able to provide.

5. Conclusion

The major key-points of the proposed approach can be summarized as in the follows:

- The procedure requires only remote sensing products, and therefore it is completely independent from ancillary ground-based measurements and benefits of the recent MODIS and MSG-SEVIRI time-series products;
- The simulated values of R_n and its components resulted consistent and comparable with the local ground measurements, therefore the procedure might be used in regions where radiation measurements are missing or limited;
- The temporal resolutions and repetitiveness of time-series products allowed to generate a robust data-base of simulated values of R_n that might be used also for gap-filling procedures of existent climate network systems;
- The model output in terms of thematic maps provided an effective way to easily estimate, at regional scale, spatial and temporal changes of one of the fundamental variables related to water resource management, agriculture, ecology and climate change.

Further research aiming at improving the proposed approach, might include a pre-elaboration procedure to take into account the quality index of MODIS products as well as the use of atmospheric emissivity and air temperature data, included in the MSG-SEVIRI product but not yet available, to increase the accuracy of the corresponding incoming long-wave radiation product analysis.

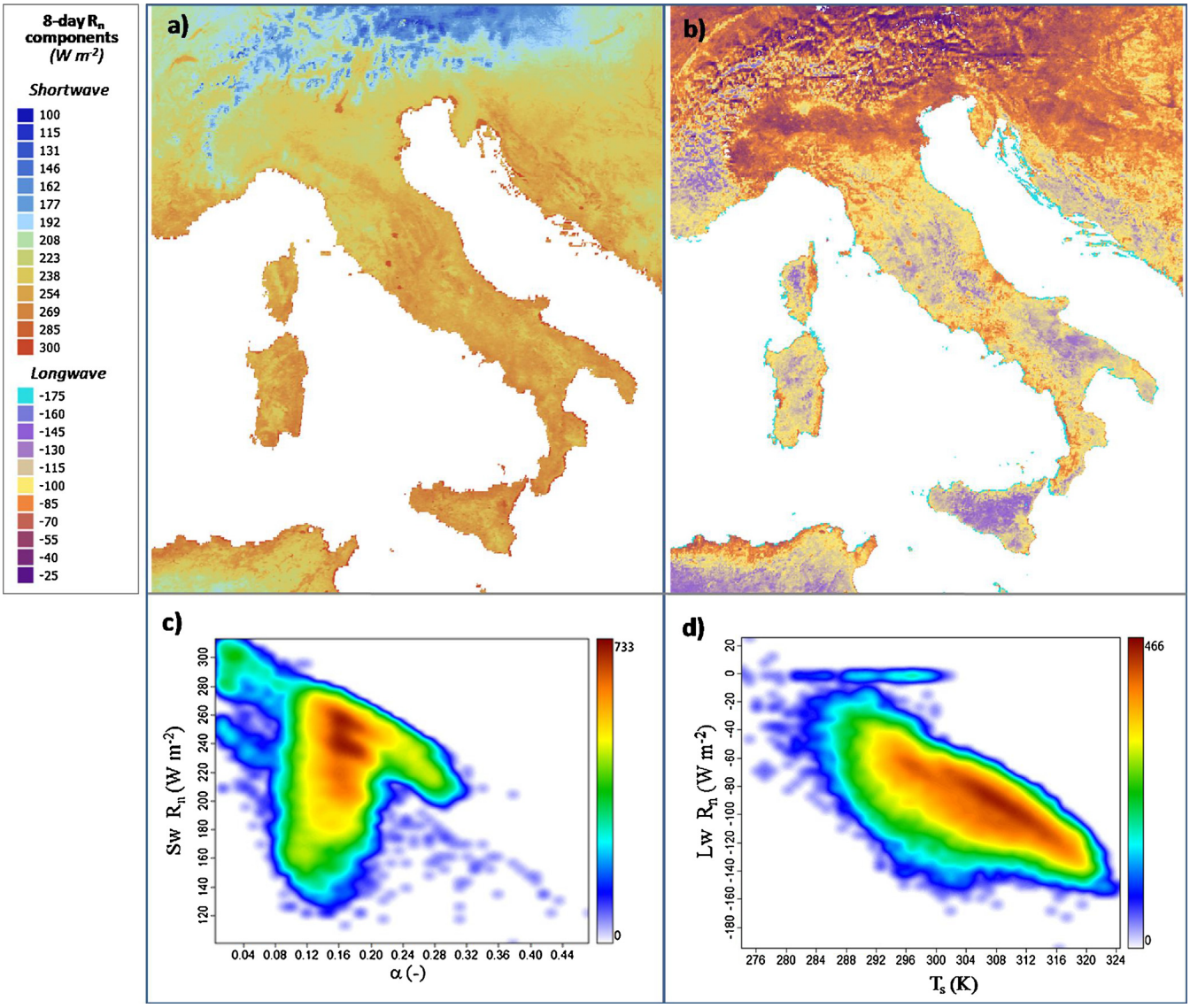

Fig. 12. Maps of shortwave (a) and longwave (b) R_n components obtained for the period 2012 August 4th–11th; density scatterplot (expressed as number of points for each coordinate pair) between α and net shortwave R_n component (c) and T_s *versus* net longwave R_n (d).

Acknowledgments

This workused eddy covariance data acquired and shared by the FLUXNET community, including these networks: CarboEuropeIP, CarboItaly, CarboMont. The ERA-Interim reanalysis data are provided by ECMWF and processed by LSCE. The FLUXNET eddy covariance data processing and harmonization was carried out by the European Fluxes Database Cluster and Fluxdata project of FLUXNET (GHG-Europe EU-FP7, EuroFlux EU-FP4, CarboEuroFluxEU-FP5).

The authors thank the EU and the Italian Ministry of Education, Universities and Research for funding, as part of the collaborative international consortium IRIDA ("Innovative remote and ground sensors, data and tools into a decision support system for agriculture water management"), financed under the ERA-NET Cofund WaterWorks 2014. This ERA-NET is an integral part of the 2015 Joint Activities developed by the Water Challenges for a Changing World Joint Programme Initiative (Water JPI). The authors also acknowledge support from the ERANET-MED project WASA ("Water Saving in Agriculture: Technological developments for the sustainable management of limited water resources in the Mediterranean area").

References

Alados, I., Foyo-Moreno, I., Olmo, F.J., Alados-Arboledas, L., 2003. Relationship between net radiation and solar radiation for semi-arid shrub-land. Agric. For. Meteorol. 116 (3–4), 221–227.

Augustine, J.A., DeLuisi, J.J., Long, C.N., 2000. SURFRAD – a national surface radiation budget network for atmospheric research. Bull. Am. Meteorol. Soc. 81, 2341–2357.

Augustine, J.A., Hodges, G.B., Cornwall, C.R., Michalsky, J.J., Medina, C.I., 2005. An update on SURFRAD – the GCOS surface radiation budget network for the continental United States. J. Atmos. Ocean. Technol. 22, 1460–1472.

Baldocchi, D., Falge, E., Gu, L.H., Olson, R., Hollinger, D., Running, S., Anthoni, P., Bernhofer, C., Davis, K., Evans, R., Fuentes, J., Goldstein, A., Katul, G., Law, B., Lee, X.H., Malhi, Y., Meyers, T., Munger, W., Oechel, W., Pilegaard, K., Schmid, H.P., Valentini, R., Verma, S., Vesala, T., Wilson, K., Wofsy, S., 2001. FLUXNET: a new tool to study the temporal and spatial variability of ecosystem-scale carbon dioxide, water vapor, and energy flux densities. Bull. Am. Meteorol. Soc. 82, 2415–2434.

Barkstrom, B.R., Smith, G.L., 1986. The earth radiation budget experiment: science and implementation. Rev. Geophys. 24, 379–390.

Bastiaanssen, W.G.M., Pelgrum, H., Wang, J., Ma, Y., Moreno, J.F., Roerink, G.J., Van der Wal, T., 1998. A remote sensing surface energy balance algorithm for land (SEBAL).: part 2: validation. J. Hydrol. (Amst.) 212, 213–229.

Bisht, G., Venturini, V., Islam, S., Jiang, L., 2005. Estimation of the net radiation using MODIS (Moderate Resolution Imaging Spectroradiometer) data for clear sky days. Remote Sens. Environ. 97, 52–67.

Blad, B.L., Walter-Shea, E.A., Mesarch, M.A., Hays, C.J., Starks, P.J., Deering, D.W., Eck, T.F., 1998. Estimating net radiation with remotely sensed data: results from KUREX-91 and FIFE studies. Remote. Sens. Rev. 17, 55–71.

Brunsell, N.A., Ham, J.M., Arnold, K.A., 2011. Validating remotely sensed land surface fluxes in heterogeneous terrain with large aperture scintillometry. Int. J. Remote Sens. 32, 6295–6314.
Carmona, F., Rivas, R., Caselles, V., 2015. Development of a general model to estimate the instantaneous, daily, and daytime net radiation with satellite data on clear-sky days. Remote Sens. Environ. 171, 1–13.
Cescatti, A., Marcolla, B., 2014. Drag coefficient and turbulence intensity in conifer canopies. Agric. For. Meteorol. 121 (3-4), 197–206.
Consoli, S., Vanella, D., 2014. Comparisons of satellite-based models for estimating evapotranspiration fluxes. J. Hydrol. (Amst.) 513, 475–489.
Consoli, S., Licciardello, F., Vanella, D., Pasotti, L., Villani, G., Tomei, F., 2016. Testing the water balance model criteria using TDR measurements, micrometeorological data and satellite-based information. Agric. Water Manag. 170, 68–80.
Cox, S.J., Stackhouse Jr., P.W., Gupta, S.K., Mikovitz, J.C., Zhang, T., Hinkelman, L.M., Wild, M., Ohmura, A., 2006. The NASA/GEWEX surface radiation budget project: overview and analysis. Proceedings of the 12th Conference on Atmospheric Radiation 10–14.
Cruz-Blanco, M., Gavilán, P., Santos, C., Lorite, I.J., 2014. Assessment of reference evapotranspiration using remote sensing and forecasting tools under semi-arid conditions. Int. J. Appl. Earth Obs. Geoinf. 33, 280–289.
Derrien, M., Le Gléau, H., 2005. MSG/SEVIRI cloud mask and type from SAFNWC. Int. J. Remote Sens. 26, 4707–4732.
Foken, T., 2008. The energy balance closure problem – an overview. Ecol. Appl. 18, 1351–1367.
Foken, T., Wimmer, F., Mauder, M., Thomas, C., Liebethal, C., 2006. Some aspects of the energy balance closure problem. Atmos. Chem. Phys. Discuss. 6, 4395–4402.
Geiger, B., Meurey, C., Lajas, D., Franchisteguy, L., Carrer, D., Roujean, J.-L., 2008. Near real-time provision of downwelling shortwave radiation estimates derived from satellite observations. Meteorol. Appl. 15, 411–420.
Gilgen, H., Ohmura, A., 1999. The global energy balance archive. Bull. Am. Meteorol. Soc. 80, 831–850.
Gockede, M., Rebmann, C., Foken, T., 2004. A combination of quality assessment tools for eddy covariance measurements with footprint modelling for the characterisation of complex sites. Agric. For. Meteorol. 127, 175–188.
Gómez, I., Caselles, V., Estrela, M.J., 2016. Seasonal characterization of solar radiation estimates obtained from a MSG-SEVIRI-Derived dataset and a RAMS-Based operational forecasting system over the Western Mediterranean coast. Remote Sens. (Basel) 8, 46.
Harding, R.J., Johnson, R.C., Soegaard, H., 1995. The energy balance of snow and partially snow covered areas in western Greenland. Int. J. Climatol. 15, 1043–1058.
Harries, J.E., Russell, J.E., Hanafin, J.A., Brindley, H., Futyan, J., Rufus, J., Kellock, S., Matthews, G., Wrigley, R., Last, A., Mueller, J., Mossavati, R., Ashmall, J., Sawyer, E., Parker, D., Caldwell, M., Allan, P.M., Smith, A., Bates, M.J., Coan, B., Stewart, B.C., Lepine, D.R., Cornwall, L.A., Corney, D.R., Ricketts, M.J., Drummond, D., Smart, D., Cutler, R., Dewitte, S., Clerbaux, N., Gonzalez, L., Ipe, A., Bertrand, C., Joukoff, A., Crommelynck, D., Nelms, N., Llewellyn-Jones, D.T., Butcher, G., Smith, G.L., Szewczyk, Z.P., Mlynczak, P.E., Slingo, A., Allan, R.P., Ringer, M.A., 2005. The geostationary earth radiation budget project. Bull. Am. Meteorol. Soc. 86, 945–960.
Hou, J., Jia, G., Zhao, T., Wang, H., Tang, B., 2014. Satellite-Based estimation of daily average net radiation under clear-sky conditions. Adv. Atmos. Sci. 31, 705–720.
Jacobowitz, H., Smith, W.L., Howell, H.B., Nagle, F.W., Hickey, J.R., 1979. The first 19 months of planetary radiation budget measurements fro the Nimbus-6ERB. J. Atmos. Sci. 36, 501–507.
Jacobowitz, H., Tighe, R.J., Arking, A., Hickey, J.R., Ingersoll, A., Maschhoff, R., Smith, G.L., Stowe, L.L., Vonder Haar, T.H., 1984. The Earth radiation budget derived from the Nimbus-7 ERB experiment. J. Geophys. Res. 89, 4997–5010.
Jacobs, A.F.G., Heusinkveld, B.G., Holtslag, A.A.M., 2008. Towards closing the surface energy budget of a mid-latitude grassland. Bound. Meteorol. 126, 125–136.
Journee, M., Bertrand, C., 2010. Improving the spatio-temporal distribution of surface solar radiation data by merging ground and satellite measurements. Remote Sens. Environ. 114, 2692–2704.
Key, J.R., Schweiger, A.J., Stone, R.S., 1997. Expected uncertainty in satellite-derived estimates of the surface radiation budget at high latitudes. J. Geophys. Res. 102 (15) 837-15,847.
Kim, J., Hogue, T.S., 2013. Evaluation of a MODIS triangle-based evapotranspiration algorithm for semi-arid regions. J. Appl. Remote Sens. 7 073493–073493.
Llasat, M.C., Snyder, R.L., 1998. Data error effects on net radiation and evapotranspiration estimation. Agric. For. Meteorol. 91, 209–221.
Marcolla, B., Cescatti, A., Manca, G., Zorer, R., Cavagna, M., Fiora, A., Gianelle, D., Rodeghiero, M., Sottocornola, M., Zampedri, R., 2011. Climatic controls and ecosystem responses drive the inter-annual variability of the net ecosystem exchange of an alpine meadow. Agric. For. Meteorol. 151 (9), 1233–1243.
Mardikis, M.G., Kalivas, D.P., Kollias, V.J., 2005. Comparison of interpolation methods for the prediction of reference evapotranspiration—an application in Greece. Water Resour. Manage. 19, 251–278.
Minacapilli, M., Consoli, S., Vanella, D., Ciraolo, G., Motisi, A., 2016. A time domain triangle method approach to estimate actual evapotranspiration: application in a Mediterranean region using MODIS and MSG-SEVIRI products. Remote Sens. Environ. 174, 10–23.
Ohmura, A., Gilgen, H., Wild, M., 1989. Global energy balance archive (GEBA) report 1: introduction. Zürcher Geographische Schriften 34, 62.
Ohmura, A., Dutton, E.G., Forgan, B., Frohlich, C., Gilgen, H., Hegner, H., Heimo, A., Konig-Langlo, G., McArthur, B., Muller, G., Philipona, R., Pinker, R., Whitlock, C.H., Dehne, K., Wild, M., 1998. Baseline Surface Radiation Network (BSRN/WCRP): new precision radiometry for climate research. Bull. Am. Meteorol. Soc. 79, 2115–2136.
Pan, X., Liu, Y., Fan, X., 2015. Comparative assessment of satellite-retrieved surface net radiation: an examination on CERES and SRB datasets in China. Remote Sens. (Basel) 7, 4899–4918.
Ramírez-Cuesta, J.M., Cruz-Blanco, M., Santos, C., Lorite, I.J., 2017a. Assessing reference evapotranspiration at regional scale based on remote sensing, weather forecast and GIS tools. Int. J. Appl. Earth Obs. Geoinf. 55, 35–42.
Ramírez-Cuesta, J.M., Kilic, A., Allen, R., Santos, C., Lorite, I.J., 2017b. Evaluating the impact of adjusting surface temperature derived from Landsat 7 ETM+ in crop evapotranspiration assessment using high-resolution airborne data. Int. J. Remote Sens. 38, 4177–4205.
Smith, W.L., Hilleary, D.T., Jacobowitz, H., Howell, H.B., Hickey, J.R., Drummond, A.J., 1977. Nimbus-6 earth radiation budget experiment. Appl. Opt. 16, 306–318.
Soltani, M., Mauder, M., Laux, P., Kunstmann, H., 2017. Turbulent flux variability and energy balance closure in the TERENO prealpine observatory: a hydrometeorological data analysis. Theor. Appl. Climatol. 1–20.
Tang, R., Li, Z.-L., Chen, K.-S., 2011. Validating MODIS-derived land surface evapotranspiration with in situ measurements at two AmeriFlux sites in a semiarid region. J. Geophys. Res. Atmos. 116 no D4.
Wan, Z., 2013. MODIS Land Surface Temperature Products User's Guide. Institute for Computational Earth System Science, University of California, Santa Barbara, CA. http://www.icess.ucsb.edu/modis/LstUsrGuide/usrguide.html.
Wielicki, B.A., Barkstrom, B.R., Baum, B.A., Charlock, T.P., Green, R.N., Kratz, D.P., Lee, R.B.I., Minnis, P., Smith, G.L., Wong, T., Young, D.F., Cess, R.D., Coakley, J.A., Crommelynck, D.A.H., Donner, L., Kandel, R., King, M.D., Miller, A.J., Ramanathan, V., Randall, D.A., Stowe, L.L., Welch, R.M., 1998. Clouds and the Earth's radiant energy system (CERES): algorithm overview. IEEE Trans. Geosci. Remote Sens. 36, 1127–1141.
Wilson, K.B., Goldstein, A., Falge, E., Aubinet, M., Baldocchi, D., Berbigier, C., Ceulemans, R., Dolman, H., Field, C., Grelle, A., Ibrom, A., Law, B., Kowalski, A., Meyers, T., Moncrieff, J., Monson, R., Oecal, W., Tenhunen, J., Valentini, R., Verma, S., 2002. Energy balance closure at FLUXNET sites. Agric For. Meteorol. 113, 223–243.
Zhang, Y., Rossow, W.B., Lacis, A.A., Oinas, V., Mishchenko, M.I., 2004. Calculation of radiative fluxes from the surface to top of atmosphere based on ISCCP and other global data sets: refinements of the radiative transfer model and the input data. J. Geophys. Res. Atmos. 109, D19105.
Zhao, L., Lee, X., Liu, S., 2013. Correcting surface solar radiation of two data assimilation systems against FLUXNET observations in North America. J. Geophys. Res. Atmos. 118, 9552–9564.
Zhou, J., Hu, D., Weng, Q., 2010. Analysis of surface radiation budget during the summer and winter in the metropolitan area of Beijing, China. J. Appl. Remote Sens. 4, 043513.